Chin. J. Astron. Astrophys. Vol. 4 (2004), No. 1, 28–36
(http://www.chjaa.org or http://chjaa.bao.ac.cn)

Chinese Journal of Astronomy and Astrophysics

The Kiloparsec–scale Structure of 3C 286 *

Tao An, Xiao-Yu Hong and Wei-Hua Wang

Shanghai Astronomical Observatory, Chinese Academy of Sciences, Shanghai 200030;
antao@center.shao.ac.cn
National Astronomical Observatories, Chinese Academy of Sciences, Beijing 100012

Received 2003 May 29; accepted 2003 August 29

Abstract We present radio images of the compact steep spectrum (CSS) quasar 3C 286 acquired with the Very Large Array (VLA) at 8.4 and 22.5 GHz. The source exhibits a two–sided core–jet structure with a bright central component and two extended components one to the east (P.A. 100°) and another to the southwest (P.A. −116°). From the compact core, an extension runs towards the southwest component up to ∼ 0.7 arcsecond. The emission between the primary central component and the southwest component exhibits a knotty structure. A gradual change of the jet position angles from −135° to −120° in the inner southwest jet suggests a local bend. The position angle changes of the major eastern components E2 and E1 suggest that the eastern jet likely follows a curved trace. The bends in the jet trace may be associated with a relativistic precession or some interaction between the jet and the ambient matter. A mean spectral index of $\alpha_{8.4}^{22.5} \sim -0.76$ ($S_\nu \propto \nu^\alpha$) is estimated for the core component. Steep spectra are also obtained for the extended southwest component (2.6″, P.A. −116°) and eastern component (0.8″, P.A. 100°), with $\alpha_{8.4}^{22.5} \sim -0.88$ and $\alpha_{8.4}^{22.5} \sim -1.79$, respectively. The radio morphologies and spectral index distributions suggest that the core seen in our images is likely to be the beamed inner jet while the real nucleus is dimmed by it beaming away from us.

Key words: galaxy: quasar: individual — radio continuum: VLA

1 INTRODUCTION

The radio source 3C 286 (1328+307) is identified with a $17^{\rm m}$ CSS quasar at a redshift $z = 0.849$ (Peacock & Wall 1982; Fanti et al. 1985). There is a foreground HI absorption line system at $z = 0.6922$ to the southeast of the quasar at a distance of $\sim 2''$ (Brown & Roberts 1973; Steidel et al. 1994). The radio spectrum is flat below 1 GHz and turnovers at about 100 MHz. It shows no distinct flux density variation on radio bands (Peng et al. 2000), but a high polarization at radio wavelengths has been detected (Akujor & Garrington 1995; Lüdke et al. 1998). It is often used as a total flux and polarization calibrator in VLA observations.

∗ Supported by the National Natural Science Foundation of China.

The VLA observation of 3C 286 at 5 GHz by Spencer et al. (1989) exhibits a kiloparsec–scale radio morphology with a secondary component located $\sim 2.6''$ to the southwest of the primary component. The Multi-Element Radio Linked Interferometer Network (MERLIN) image at 1.6 GHz presented in the same paper exhibits a non–linear triple structure with a size of $\sim 3.8''$ in the east–west direction with two secondary components, one at $2.6''$ to the southwest (P.A. $\sim -115°$) and one at $0.8''$ to the east (P.A. $\sim 100°$). The triple structure is also obtained in high dynamic range VLA images at 5 GHz by Hines, Owen & Eilek (1989) and at 8.4 GHz by Akujor & Garrington (1995). A collimated jet starts from the core and leads towards the southwest component with a local gap around $0.8''$.

A one–sided core–jet structure on parsec scales is displayed in 3C 286. The jet extends to the southwest from the core with a major curvature at ~ 75 mas from P.A. $= -138°$ to P.A. $= -120°$ (Zhang et al. 1994 and references in it). A MERLIN polarimetric observation by Lüdke et al. (1998) also detected this curvature at ∼75 mas from the core. Moreover, the results show that the angle of polarization changes where the jet bends. The Very Long Baseline Interferometry (VLBI) polarimetric observations detected high polarization and perpendicular magnetic field in the VLBI core and the inner 70–mas jet (Akujor & Garrington 1995; Dallacasa et al. 1996; Jiang et al. 1996; Cotton et al. 1997).

One of the most significant observational results from the Energetic Gamma–Ray Experiment Telescope (EGRET), on board the Compton Gamma Ray Observatory (CGRO), is the detection of high energy γ–ray emission from more than 66 active galactic nuclei (AGNs) (Fichtel et al. 1994; Thompson et al. 1995; Mukherjee et al. 1997; Hartman et al. 1999). To better understand the observational properties of EGRET–detected AGNs on kpc scales, we observed a sample of 15 EGRET–detected AGNs with VLA at 8.4 and 22.5 GHz (Hong et al. 2003). We also observed 3C 286 as a phase calibrator in the VLA observations. In the next section, the VLA observations and data reduction are briefly introduced. The image analysis of the high dynamic range VLA images of 3C 286 at 8.4 and 22.5 GHz is described in Sect. 3. In Sect. 4, the radio structure of 3C 286, based on the radio morphologies and spectral index distribution, is discussed, and a summary is given in the last section.

2 OBSERVATIONS AND DATA REDUCTION

We observed 3C 286 with dual frequency (8.4/22.5 GHz) VLA in C–configuration (the longest baseline is 3.6 kilometer) on 1999 January 29 (1999.08) and obtained radio images with sub–arcsecond resolutions. We found that 3C 286 was not resolved at 8.4 GHz and slightly resolved at 22.5 GHz. To acquire higher resolution images we re-observed 3C 286 with VLA at the same frequencies in A–configuration on 2000 December 1 (2000.92). The longest baseline in the A–configuration is 36 km, 10 times the resolution in the C–configuration. The faint extended emission is clearly resolved on the longer baselines at the later epoch 2000.92. The observed results are exhibited in the next section. The dual frequency data also enabled us to make a spectral analysis of the observed source.

The observations were carried out in the snapshot mode with a bandwidth of 50 MHz. The absolute flux densities for the EGRET–blazar sources were calibrated by observing the primary calibrator 3C 48 for 7 minutes at the beginning of the run at each frequency. The secondary calibrator 3C 286 was observed for 2 minutes every hour during the observations to track the phase errors. The amplitude and phase calibrations of the 1999.08 C–configuration dataset were based on the dataset itself. The source was clearly resolved in the VLA A–configuration

at the epoch 2000.92 at both frequencies. To avoid flux calibration errors, another unresolved calibrator, 3C 48, was used as the amplitude and phase calibrator when calibrating the A–configuration dataset. The ultimate calibration errors are believed to be less than 3% for each single dataset.

The data reduction, including editing, amplitude and phase calibration, and imaging analysis were done in NRAO $\mathcal{AIPS}$ (Astronomical Image Processing System) and DIFMAP (DIFference MAPping) packages (Shepherd, Pearson & Taylor 1994). The observational epoch, frequency, array configuration and the maximum baseline are listed in Cols.2 to 5 of Table 1.

Table 1 Observational Log and Particulars of Contour Maps

Figure	Epoch	Freq (GHz)	Array	$UV_{\rm max}$ (km)	Restored Beam (arcsec)	$S_{\rm peak}$ (Jy/b)	rms (mJy/b)	Contours (mJy/b)
(1)	(2)	(3)	(4)	(5)	(6)	(7)	(8)	(9)
Fig. 1a	1999.08	22.5	VLA C	3.6	0.88×0.81, -7.1°	2.5	0.35	$0.9 \times (-1, 1, 2...1024)$
Fig. 1b	2000.92	8.4	VLA A	36	0.26×0.23, -20.8°	5.1	0.23	$0.76 \times (-1, 1, 2...1024)$
Fig. 1c	2000.92	22.5	VLA A	36	0.10×0.09, 0.0°	2.6	0.29	$0.9 \times (-1, 1, 2...512)$

3 ANALYSIS OF THE IMAGES

The VLA hybrid images of 3C 286 at three different resolutions are displayed in Fig. 1. The C–configuration VLA image at 8.4 GHz is not shown, because it is unresolved. The restored beam, peak intensity, rms level and contour levels are listed in Columns 6 to 9 of Table 1. To quantitatively study the radio structure, we fit the two VLA A–configuration datasets at the epoch 2000.92 with several Gaussian components. Table 2 lists the parameters of the major components shown in Fig. 1b and Fig. 1c: Columns 1 and 2, the observing epoch and frequency; Column 3, the component label (the presumed core, signed with C hereafter); Columns 4 to 6, the integrated flux density, the separation and position angle of the component; Columns 7 to 9, the major axis, the axis ratio and the orientation of the major axis of the Gaussian component. Except for the core component C, the jet components are all fitted with circular Gaussian models.

The C–configuration VLA image at 22.5 GHz reveals that 3C 286 is slightly resolved. The result (Fig. 1a) shows a core–jet structure at a sub–arcsecond (0.88×0.81 arcsec) resolution. The primary component (labelled "Primary" in Fig. 1a) dominates most of the flux density and a western component (labelled "Western") is located at a distance of $\sim 2.6''$ in P.A. -116°. A continuous jet links the two.

Figure 1b is obtained with the A–configuration image at 8.4 GHz and contains more structural information. It clearly exhibits a non–linear triple structure at a resolution of 0.26×0.23 arcsec. The "Primary" component in Fig. 1a is here resolved into two components, labelled "Central" and "Eastern". The model fitting results show the "Central" component can be fitted with three sub–components: a compact core (C) and two southwest jet components labelled J2 and J1. More than 95% of the total flux in Fig. 1b is concentrated in the core C. The jet component J2 lies near the core, at $r = 0.09''$ in P.A. -128°. The other jet component, J1, is located at $r \sim 0.35''$, the southwestern extension from the core starts at P.A. $= -120^\circ$. The jet runs in the southwestern direction along P.A. -120° from the component J1 up to a distance of $\sim 0.7''$. The extended emission is strongly resolved on the longer baselines of Fig. 1b. Due to the dynamic range limit, the region between the southwestern jet and the Western component

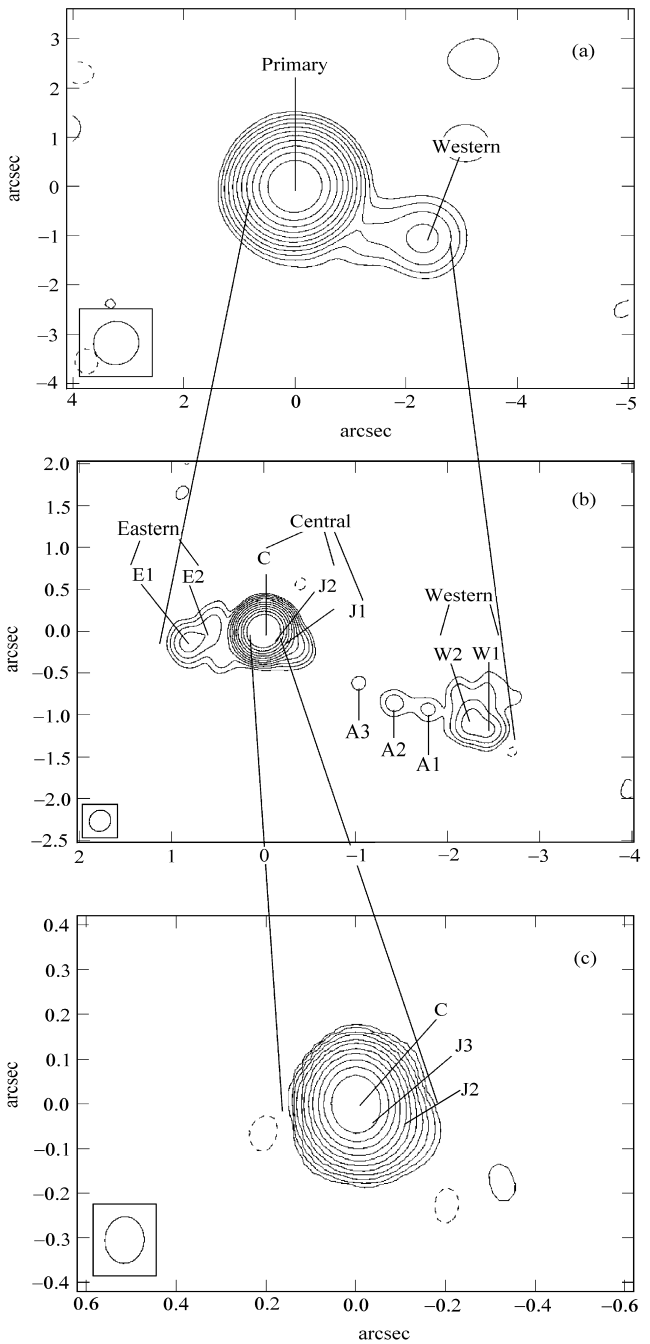

Fig. 1 Total intensity image of 3C 286. The beam size, peak flux density, off-source rms level and contour levels are listed in Columns 6–9 of Table 1. (a) VLA C–configuration observation at 22.5 GHz at epoch 1999.08; (b) VLA A–configuration observation at 8.4 GHz at epoch 2000.92; (c) VLA A–configuration observation at 22.5 GHz at epoch 2000.92.

is occupied by a series of discrete knots (Labelled as A3, A2 and A1, from east to west). They are too weak to be fitted with Gaussian models. The Western component is resolved into two sub–components, labelled W1 and W2. They align well with the southwestern jet. The "Eastern" component, at $r = 0.8''$ in P.A. 100°, is also resolved into two sub–components, E1 and E2. Between the core and E1 the morphology shows a modest bend around E2.

We noticed that most of the flux density in Fig. 1b is contained in the compact core. The core is so bright that it makes the extended emission difficult to detect. To make the faint extended structure more visible, we (1) subtract a 5-Jy δ–component from the core C using $\mathcal{AIPS}$ task *UVSUB*; (2) set a 0.3 gaussian taper in imaging to weight down the long baselines, thereby increasing the signal to noise ratio of the extended emission and reducing the sidelobes. Figure 2 shows the new enhanced image. The knots A1, A2 and A3 are embedded in a continuous jet in P.A. −120°. The Eastern and Western components become more extended.

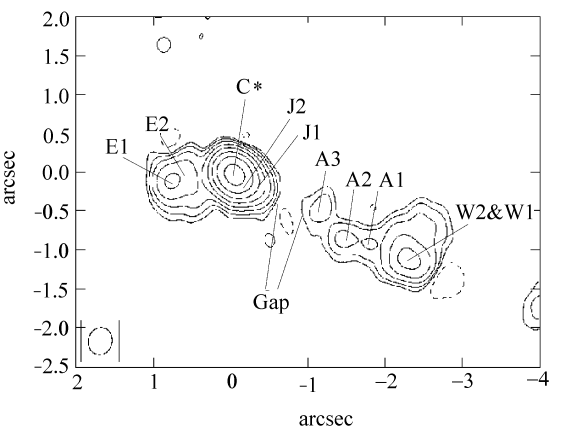

Fig. 2 Tapered image from Fig. 1b. The component C∗ means that a 5 Jy δ–component has been subtracted from the core. The beam size is 0.35×0.31 arcsec. The contour levels are $0.7 \times (-1, 1, 2, ..., 128)$ mJy/b.

Table 2 Parameters of the Gaussian Components

Epoch	Freq (GHz)	Comp	S (mJy)	R (arcsec)	θ (°)	a (mas)	b/a	P.A. (°)	Figure
(1)	(2)	(3)	(4)	(5)	(6)	(7)	(8)	(9)	(10)
2000.92	8.4	C	5000	0	0	33	0.17	45	Fig. 1b
		J2	158	0.09	–128	25	1	90	
		J1	23	0.35	–120	138	1	–90	
		E2	15	0.57	92	180	1	–90	
		E1	23	0.83	103	110	1	–85	
		W2	23	2.50	–116	250	1	–80	
		W1	8	2.76	–116	65	1	91	
2000.92	22.5	C	2370	0	0	10	0.49	44	Fig. 1c
		J3	315	0.04	–135	5	1	–73	
		J2	33	0.09	–128	10	1	–80	

The outer extended emission in Fig. 1c is well resolved, and the "Central" component is shown to have a size of $< 0.4''$ at a resolution of $0.10'' \times 0.09''$. The mission was fitted with three components and a new component J3 appears at $r = 0.04''$ in P.A. $-135°$, between the core C and the jet component J2.

4 DISCUSSION

4.1 The Source's Morphology

Our high dynamic range VLA A-configuration image of 3C 286 at 8.4 GHz (Fig. 1b) displays a well defined two–sided core–jet structure. The southwestern jet traces a linear path to a lobe at $2.6''$. Comparing the position angles of the innermost southwestern jet components, J3 ($-135°$), J2 ($-128°$) and J1 ($-120°$), we find a gradual bend from the innermost portion outwards. This bend is supported by the published VLBI observations (Lüdke et al. 1998; Kellermann et al. 1998; Fey & Charlot 2000) in which the inner jet has a bend at 75 mas from P.A. $= -135°$ to P.A. $= -120°$. After this bend the jet extends along P.A. $= -120°$ up to a "Gap" at $\sim 0.8''$. An emission bridge, embedded with three knots, starts at $r \sim 1''$ and traces the inner southwestern extension up to the "Western" component. The eastern jet is shorter than the southwestern one. Its ridge line displays a bend around the component E2 from P.A. $\sim 90°$ to P.A. $\sim 100°$.

Zhang et al. (1994) detected two flat–spectrum components with global VLBI observations. The two components are of equal brightness and are separated by $\sim$ 6 mas. The authors suggested that 3C 286 probably has two nuclei. If so, the changes of the jet position angle in 3C 286 may be associated with relativistic precession of the central engine. Alternatively, Kelvin–Helmholtz (K–H) instabilities at the jet base probably result in wiggles in extragalactic jets (Hardee, Cooper & Clarke 1994). For example, Lobanov & Zensus (2001) found a double helical structure in 3C 273 associated with K–H instabilities extending from 30 mas to sub–arcseond scales. In addition, jet–ISM interaction may be responsible for local bends in extragalactic jets. Mantovani et al. (1998) estimated that in more than 10% of CSSs jets are possibly deflected by dense clouds. We note that the polarization angle changes at the bending position around 75 mas from the core (Lüdke et al. 1998). It is possible that the mas–scale jet is reflected in the interface between the jet and the ISM where the jet bends ($\sim$75 mas from the core). The observational study of the gas environment of this CSS sources is essential for a better understanding of the radio morphologies.

4.2 Spectral Index Distribution

The source showed no flux density variation between the two observation sessions. The dual frequency observations allow us to study the spectral index distribution ($S_\nu \propto \nu^\alpha$) of 3C 286 on kpc scale. Figure 1a (22.5 GHz, VLA C–configuration) and Fig. 1b (22.5 GHz, VLA 8.4 GHz A–configuration) are observed with different array configurations. Difference in resolution does not allow a direct derivation of the spectral index of the individual components. We therefore re-imaged Fig. 1a and Fig. 1b and restored the clean images with a $0.45'' \times 0.45''$ beam. In so doing, we obtained images more resolved than Fig. 1a and less resolved than Fig. 1b; the two images have the same angular resolution and exhibit a similar radio structure (see the contour image in Fig. 3). The spectral index analysis is preformed based on the two re-imaged figures using the $\mathcal{AIPS}$ task *COMB* and the result is exhibited in Fig. 3. The wedge at the top gives the grey scale of the spectral index with dark for steep spectrum. We find an overall steep spectrum for the source. The mean spectral index of the "Central" component is estimated

as -0.75 ± 0.02 between 8.4 GHz and 22.5 GHz. The spectrum of the "Western" component is slightly steeper with $\alpha = -0.88 \pm 0.14$. The "Eastern" component, mainly the component E1 and E2, has a markedly steep spectrum with $\alpha = -1.79 \pm 0.24$.

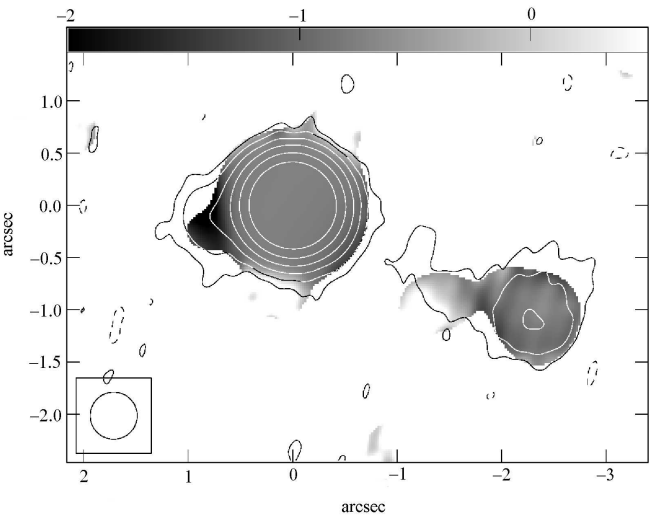

Fig. 3 Overlay of the spectral index distribution (grey) and the radio intensity image (contour). The spectral index is estimated from Fig. 1a and Fig. 1b. The restored beam is 0.45×0.45 arcsec. The contour image is re-imaged from Fig. 1b, and the contours increase in steps of 3 units from 3 mJy/b. Spectral index wedge at the top, the dark end corresponds to steep spectrum.

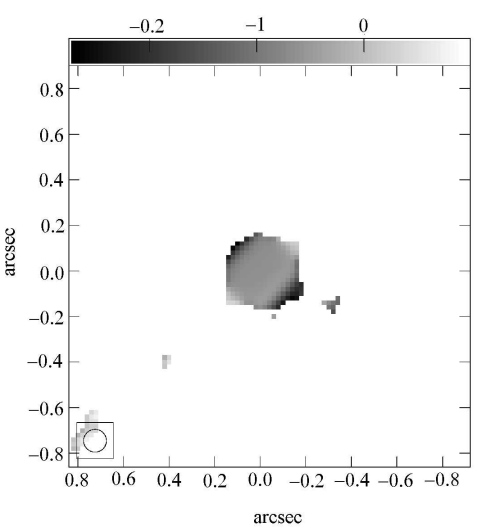

Fig. 4 Grey–scale image of the spectral index distribution in the innermost region of 3C 286. The spectral index is estimated from Fig. 1b and Fig. 1c. The restored beam is 0.1×0.1 arcsec. Same spectral index wedge as in Fig. 3.

Figure 1b (8.4 GHz, VLA A–configuration) and Fig. 1c (22.5 GHz, VLA A–configuration) are simultaneous and have the same uv-coverage. We can analysis the spectral index distribution directly from them. We note that the faint extended emission in Fig. 1c is strongly resolved, so we only exhibit the spectrum of the central $0.4''$ region within in Fig. 4. The mean spectral index between 8.4 GHz and 22.5 GHz in Fig. 4 is estimated to be $\alpha = -0.65 \pm 0.15$. The spectral index of the core (component C) in the same range estimated directly from the model fitting results (Table 2) is $\alpha_{8.4}^{22.5} = -0.76$. Noting the general agreement amount the estimates, we consider 3C 286 to have a steep–spectrum core with a mean spectral index $\alpha \sim -0.76$, as is distinguished with typical core–dominated QSO (CDQ) nuclei. This suggests that the brightest component C in our images is possibly not the real nucleus.

4.3 Relativistic Effects

Ghisellini et al. (1993) made a comprehensive study of the beaming indicators of relativistic bulk motions in AGNs. In the relativistic beaming scheme, the core emission of core-dominate quasars is possibly Doppler boosted due to beaming in our direction. The core dominance (the core/extended flux ratio R on arcsecond scales) should be a beaming indicator. Ghisellini et al. (1993) reported a statistically mean value of $\log(R)$ for CDQs, $\log(R) = 1.46 \pm 0.12$. The core dominance parameter for 3C286 estimated from Fig. 1b, is $\log(R) > 1.3$, and it falls inside the range. The presence of relativistic effects in the two–sided jets could also be evaluated by analyzing the jet/counter–jet brightness ratio J by $J = (1 + \beta\cos\theta)^{2-\alpha}(1 - \beta\cos\theta)^{-2+\alpha}$, where β and θ are the jet speed and angle to the line of sight, α is the average spectral index of the jet, here assumed to be -0.7. We assume the speeds are identical for the jet (the southwest jet) and the counter–jet (the eastern jet). We obtain a $J \sim 1.4$ from Fig. 1b, which gives $\beta\cos\theta \sim 0.07c$. Taking a median viewing angle of 30°, we evaluate the jet speed to be $\beta \sim 0.08$. The result does not support a relativistic beaming in the extended kpc–scale jet. The core dominance suggests the emission from the core (including the innermost jet) is beamed towards us, while the jet/counter–jet ratio supports the extended jet on kpc scales being aligned along the galactic plane. The brightest component C in 3C 286 is in marked disagreement with typical QSO nuclei: the spectral index ($\alpha_{8.4}^{22.5} \sim -0.76$) shows it to have a steep spectrum. Moreover, previous polarimetric observations have detected a high degree of polarization in the core C and the magnetic field is perpendicular to the jet axis from the innermost jet out to a distance of 200 mas from the core (Akujor & Garrington 1995; Lüdke et al. 1998). Cotton et al. (1997) proposed an interpretation in which a highly relativistic jet is initially beamed away from us and then curves round through the line of sight. The portion of the jet in our direction is brightened by Doppler boosting while the true nucleus is being obscured. It is probable that the core we see is not the real nucleus, but the Doppler boosted inner jet.

5 SUMMARY

The VLA image of 3C 286 in the present paper exhibits a two–sided core–jet structure. The jet to the southwest keeps collimated up to a lobe at $2.6''$ in P.A. $-116°$. The inner southwest jet displays a gradual bend from $-135°$ to $-120°$ within $0.4''$ from the core. The east jet ends in a lobe at $0.8''$ in P.A. 100°. The ridge line of the east jet has a modest bend at $\sim 0.6''$ from P.A. $\sim 90°$ to P.A. ~ 100. The bending is probably due to either K–H instability in jet flow, relativistic precession in a double nucleus system, or jet–ISM interaction. We have found an overall steep spectrum for the source. The compact steep spectrum core (with $\alpha_{8.4}^{22.5} \sim -0.76$)

dominates more than 95% of the total flux density. The core dominance suggests the emission of the core is Doppler boosted due to the beaming effect. The extended southwestern and the eastern jets have no significant difference in flux density and the derived jet/counter–jet ratio indicates that the extended kpc–scale jet is non–relativistic. The results support that the core C shown in our images is in fact the beamed innermost portion of the jet, while the real nucleus is possibly dimmed by it beaming away from us.

Acknowledgements This research was supported by the National Natural Science Foundation of China (19973103). The authors are grateful to the staff of the VLA for the support of the observing projects. This work has made use of NASA Astrophysics Data System Abstract Service.

References

Akujor C. F., Garrington S. T., 1995, A&AS, 112, 235
Brown R. L., Roberts M. S., 1973, ApJ, 184, L7
Cotton W. D., Fanti C., Fanti R. et al., 1997, A&A, 325, 479
Dallacasa D., Schilizzi R. T., Sanghera H. S. et al., 1996, IAUS, 175, 85
Fanti C., Fanti R., Parma P. et al., 1985, A&A, 143, 292
Fey A. L., Charlot P., 2000, ApJS, 128, 17
Fichtel C. E., Bertsch D. L., Chiang J. et al., 1994, ApJS, 94, 551
Ghisellini G., Padovani P., Celotti A., Maraschi L., 1993, ApJ, 407, 65
Hardee P., Cooper M., Clarke D., 1994, ApJ, 424, 126
Hartman R. C., Bertsch D. L., Bloom S. D. et al., 1999, ApJS, 123, 79
Hines D. C., Owen F. N., Eilek J. A., 1989, AJ, 347, 713
Hong X. Y., Wang W. H., An T. et al., 2003, in preparation
Jiang D. R., Dallacasa D., Schilizzi R. T. et al., 1996, A&A, 312, 380
Kellermann K. L., Vermeulen R. C., Zensus J. A., Cohen M. H., 1998, AJ, 115, 1295
Lobanov A. P., Zensus J. A., 2001, Sci, 294, 128
Lüdke E., Garrington S. T., Spencer R. E. et al., 1998, MNRAS, 299, 467
Mantovani F., Junor W., Bondi M. et al., 1998, A&A, 332, 10
Mukherjee R., Bertsch D. L., Bloom S. D. et al., 1997, ApJ, 490, 116
Peacock J. A., Wall J. V., 1982, MNRAS, 200, 1067
Peng B., Kraus A., Krichbaum T. P., Witzel A., 2000, A&AS, 145, 1
Shepherd M. C., Pearson T. J., Taylor G. B., 1994, BAAS, 26, 987
Spencer R. E., McDowell J. C., Charlesworth M. et al., 1989, MNRAS, 240, 657
Steidel C. C., Pettini M., Dickinson M., Persson S. E., 1994, AJ, 108, 2046
Thompson D. J., Bertsch D. L., Dingus B. L. et al., 1995, ApJS, 101, 259
Zhang F. J., Spencer R. E., Schilizzi R. T. et al., 1994, A&A, 287, 32